Analytica Chimica Acta 1331 (2024) 343305

Contents lists available at ScienceDirect

Analytica Chimica Acta

journal homepage: www.elsevier.com/locate/aca

Intensity- and time-based strategies for micro/nano-sizing *via* single-particle ICP-mass spectrometry: A comparative assessment using Au and SiO_2 as model particles

Antonio Bazo, Eduardo Bolea-Fernandez, Ana Rua-Ibarz, Maite Aramendía **, Martín Resano *

University of Zaragoza, Department of Analytical Chemistry, Aragon Institute of Engineering Research (I3A), Zaragoza, 50009, Spain

HIGHLIGHTS

- Critical comparison of different SP-ICP-MS methodologies for MNP sizing.
- Analytical signals based on both integrated intensities and transit times evaluated.
- The particle frequency method provided larger uncertainties than the particle size.
- TE-independent approaches displayed better precision than TE-dependent ones.
- The time-based method is suitable for sizing AuNPS but not the largest SiO_2MNPs.

GRAPHICAL ABSTRACT

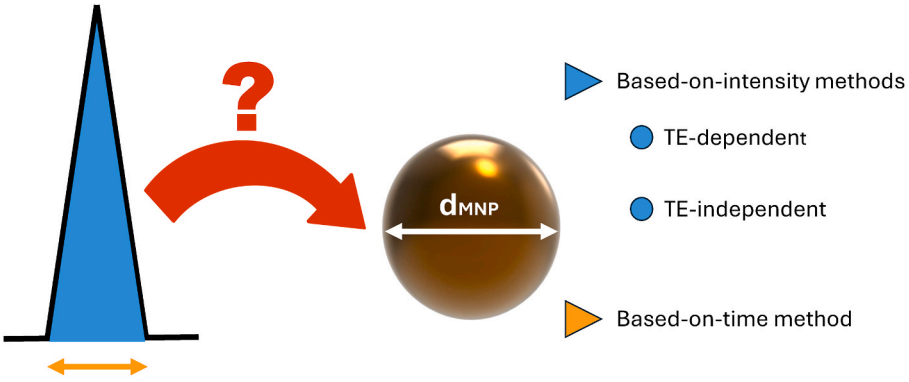

ARTICLE INFO

Handling Editor: Xiu-Ping Yan

Keywords:
Micro/nano-particles
Sizing
Single-particle ICP-Mass spectrometry (SP-ICP-MS)
Transport efficiency
Transit time
Data processing

ABSTRACT

Background: Single-particle ICP-mass spectrometry (SP-ICP-MS) is a powerful method for micro/nano-particle (MNP) sizing. Despite the outstanding evolution of the technique in the last decade, most studies still rely on traditional approaches based on (1) the use of integrated intensity as the analytical signal and (2) the calculation of the transport efficiency (TE). However, the increasing availability of MNP standards and advancements in hardware and software have unveiled new venues for MNP sizing, including TE-independent and time-based approaches. This work systematically examines these different methodologies to identify and summarize their strengths and weaknesses, thus helping to determine their preferred application areas.

Results: Different SP-ICP-MS methods for MNP sizing were assessed using AuNPs (20–70 nm) and SiO_2MNPs (100–1000 nm). Among TE-dependent approaches, the particle frequency method was characterized by larger uncertainties than the particle size method. The results of the latter were dependent on the appropriate selection of the reference MNP, making the use of multiple reference MNPs recommended. TE-independent methods were based on external (linear and polynomial) calibrations and a relative approach. These methods exhibited the lowest uncertainties of all the strategies evaluated. External calibrations benefited from simpler calculations, but their application could be hindered by a lack of reference MNPs within the desired size range or by the need for

* Corresponding author.
** Corresponding author.
E-mail addresses: maiteam@unizar.es (M. Aramendía), mresano@unizar.es (M. Resano).

https://doi.org/10.1016/j.aca.2024.343305
Received 8 July 2024; Received in revised form 13 September 2024; Accepted 4 October 2024
Available online 5 October 2024

interpolations outside the calibration range. Finally, transit time signals are directly proportional to the MNP size rather than its mass. The time-based method demonstrated adequate performance for sizing AuNPs but failed when sizing the largest SiO_2MNPs (1000 nm).

Significance and novelty: This work provides further insights into the application of different SP-ICP-MS methodologies for MNP sizing. Both TE-independent approaches and the monitoring of the transit time as the analytical signal are underused strategies; in this context, a Python script was developed for accurate transit time measurement. After 20 years of development, a quantitative comparison of the different methodologies, including the most novel approaches, is deemed necessary for further growth on solid theoretical ground.

1. Introduction

Micro- and nano-particles (MNPs) exhibit distinct size-dependent properties as compared to their larger-scale counterparts. Therefore, obtaining reliable information on the size of MNP populations is crucial for various fields, including environmental monitoring [1–3], food [4,5], and life sciences [6], among others. While several analytical techniques have already been used for the size determination of MNPs, single-particle inductively coupled plasma-mass spectrometry (SP-ICP-MS) has been identified as an emerging technology that can provide comprehensive information on thousands of MNPs in a short timeframe, even at the very low concentration levels at which these are often found in real samples [7,8]. When operated in SP mode, every individual particle introduced into the ICP ion source gives rise to a very short transient signal. Adequate calibration and data processing provide information on the elemental composition, the dissolved analyte concentration, the particle number concentration (PNC), and the mass and size distributions [9–12].

Since the first application of SP-ICP-MS in 2003 [9], the popularity of this technique has grown very rapidly. However, the data treatment of fast temporally resolved signals remains challenging. To address this, various strategies are being proposed to convert the individual signal spikes generated by MNPs, the so-called single events, into mass. The mass can then be used to determine the size, on the condition of well-known MNP density, shape, and chemical composition. These strategies typically make use of the integrated intensity of every individual event as the analytical signal. On the other hand, recent advances in the instrumentation have opened new possibilities by acquiring ultrafast temporally resolved information (up to 100,000 read-outs per second), allowing for the accurate monitoring of the transit time (temporal width) of the events [13,14]. It should be noted that Duffin et al. [15] and Schardt et al. [16] proposed using external data acquisition units to obtain temporal information even faster (ns temporal resolution), but the present work only relates to the approaches that can be used with commercially available state-of-the-art ICP-MS instrumentation. Overall, SP-ICP-MS methods can currently be classified into based-on-intensity and based-on-time approaches, depending on the selected analytical signal.

Time-based methods have been used to obtain information on the aspect ratio of anisotropic nanostructures (nanorods) [13] and the elemental distribution of bimetallic NPs [14], but their application to MNP size determination is still in its infancy. It is important to note that, for time-based methods, the analytical signal (time) is directly related to the MNP size rather than its mass, making it a direct approach for determining MNP size. In short, the procedure is based on the linear relationship between transit time and MNP size, which allows for the interpolation of the duration of sample events in a calibration curve constructed from MNP standards of well-known size and of the same density and chemical composition as that of the target MNPs. Moreover, time-based approaches do not rely on the calculation of a transport efficiency factor (TE) for MNP size determination. On the other hand, intensity-based approaches can be subcategorized depending on whether they require the determination of the TE or not.

Transport efficiency-dependent approaches use a calculable proportionality constant (TE) that correlates the intensity of MNP events with their mass [17,18]. Several methods have been proposed to determine this factor [19,20], but the most commonly used ones (which will be evaluated in this work) rely on using an MNP standard with a well-known property that can be mathematically correlated to a measurand through the TE. Depending on the standardized property, two different approaches can be distinguished: the particle size method, which correlates the mass of the MNP standard (calculated from its reference size) to the mean intensity of the events detected for such a standard, and the particle frequency method, which associates the PNC of the MNP standard with the number of events detected. Further details of these calculations can be found in Section 2.3.1.

On the other hand, there are other intensity-based methods that do not require the calculation of the TE, but that still require the analysis of MNP standards of well-known size. The first approach to mention is probably the most intuitive one and simply consists of constructing a calibration curve with MNP standards by plotting their mean intensity versus their particle mass (lineal relationship) or size (third-degree relationship) so the intensity of the sample events can be interpolated in the respective calibration curve to derive their mass or size [21]. Surprisingly, this approach is only rarely used, although perhaps this can be explained based on the rather limited availability of MNP standards at the time when the technique was developed. This approach will be referred to as direct external calibration, indicating that no TE needs to be estimated.

The second method was recently proposed by Moreira-Álvarez et al. [22], and is based on analyzing an ionic standard solution, an MNP standard, and a sample under different instrument sensitivity conditions so that the mass of the MNP sample can be correlated to their relative variations of intensity. This method is further described in Section 2.3.1. and will be referred to as relative approach, following the nomenclature introduced in Ref. [22].

All methods described above exhibit different analytical features, and distinct advantages and disadvantages that need to be carefully evaluated prior to appropriate selection. Therefore, this work systematically examines all the methodologies discussed above for sizing MNPs, some very common and some very seldom reported before, in order to identify and summarize their strengths and weaknesses, thus helping to identify their preferred areas of application. After approx. 20 years of development of SP-ICP-MS, such comparison is still missing, and it is deemed necessary for further growth on solid theoretical ground. For this purpose, the performance of the abovementioned different methods was experimentally evaluated. As model MNPs, both small (20–70 nm), metallic, and high-density AuNPs, as well as big (80–1000 nm), non-metallic, and low-density SiO_2MNPs, were targeted.

2. Materials and methods

2.1. Reagents, standards, and samples

Analytical purity grade reagents were used throughout this work. Ultra-pure water (resistivity >18.2 MΩ cm) was obtained from a Milli-Q water purification system (Millipore, Molsheim, France). The performance of the methods for size determination was evaluated using the following aqueous suspensions: 30 and 50 nm Ultra Uniform™ AuNPs (Nanocomposix Europe, Praque, Czech Republic), 20, 40, 60, and 70 nm

Table 1
ICP-MS operating conditions.

Measurement conditions	
RF Power, W	1600
Nebulizer gas flow, L min^{-1}	1.01
Plasma gas flow, L min^{-1}	16
Auxiliary gas flow, L min^{-1}	1.2
Detection mode	Q3 Only
Dwell time, μs	100 [a]
Acquisition time, s	100
CRC Mode	No gas (Au), 0.9 mL min^{-1} H_2 (Si)
Rpq	0.25
Instrumental setup	
Sample introduction system	Quartz cyclonic spray chamber Type A concentric nebulizer
Sampling tube internal diameter, mm	0.38
Uptake rate, mL min^{-1}	0.21
Introduction system	Peristaltic pump
NP parameters for calculations	
AuNP density, g cm^{-3}	19.32
SiO_2MNP density, g cm^{-3}	2.65

[a] Except for time-based methods, for which different dwell times were evaluated as discussed in section 3.2.

AuNPs (HiQ-Nano, Arnesano, Italy), and 100, 120, 200, 500, and 1000 nm SiO_2MNPs (Nanocomposix Europe). The reference material Colloid gold nanoparticles - nominal diameter 30 nm (Quality Control Material LGCQC5050; 32.7 ± 2.0 nm), also available as an aqueous suspension, was measured as well. Appropriate dilutions of the original MNP suspensions were prepared in ultra-pure water.

For method development and calibration purposes, 1 g L^{-1} single-element standard solutions of Au and Si (Merck, Darmstadt, Germany) were respectively diluted in 0.6 M HCl and 0.14 M HNO_3 solutions prepared from 12 M HCl and 14 M HNO_3 stock standard solutions (Merck, Darmstadt, Germany). To overcome the occurrence of spectral interferences originating from $(^{12}C^{16}O)^+$ and $(^{14}N^{14}N)^+$ on $^{28}Si^+$, the collision/reaction cell (CRC) was pressurized with H_2 gas (Nippon Gases, Madrid, Spain).

2.2. Instrumentation

All measurements were carried out using a NexION 5000 (PerkinElmer, Waltham, MA, USA) ICP-MS/MS instrument. The sample introduction system comprises a concentric quartz nebulizer (0.4 mL min^{-1}) and a quartz cyclonic-type spray chamber. The triple cone interface with OmniRing™ was operated in extraction mode to achieve the maximum sensitivity. The instrument is equipped with a quadrupole ion deflector (QID; Q0) that selectively focuses the ion beam over a 90-degree angle, prior to introduction into the mass spectrometer (MS). The MS consists of two additional quadrupole mass analyzers (Q1 and Q3; <0.7 amu mass resolution) and a quadrupole collision/reaction cell (CRC; Q2) mounted in between. In this work, the instrument was operated in single-quadrupole or "Q3 Only" mode, so that the first full-sized resolving quadrupole (Q1) was fully open. Daily performance checks were carried out to optimize the torch position, QID, and nebulizer gas settings, so that the instrument sensitivity was maximized while keeping the $Ce^{++}(70)/Ce^{+}(140)$ and $CeO^{+}(156)/Ce^{+}(140)$ ratios equal or under 0.03 and 0.025, respectively. Additional instrument settings and data acquisition parameters are summarized in Table 1. For SP-ICP-MS analysis and preliminary data visualization, the instrument is equipped with the Syngystix Nano Application module (v3.5). For statistical evaluation, interpolations, plots, and fittings, the OriginPro software (version 2021b, 9.85) was used. Intensity signals were fitted to Gaussian distributions, and their central value (I_c) was chosen as the analytical signal, whereas the mean value was selected for the time signals, for which not every distribution could be fitted to a Gaussian function, as will be discussed in Section 3.2.

2.3. Measurement protocol

2.3.1. Analysis and calibration

To ensure a proper comparison of the different methods and avoid bias from measurement uncertainty, the SP-ICP-MS dataset was collected within a single measurement session. During this session, all MNP dispersions were analyzed once to be able to perform the measurements in the shortest period of time for the fairest possible comparison, and both their intensity and transit time distributions were obtained. Nevertheless, it has to be understood that each and every replicate represents the quantification of more than 2000 individual MNPs. Each MNP standard was treated both as a sample and as a standard for determining the size of the other MNPs, as will be discussed later. Consequently, the same dataset was used for inter-method comparison, and all calculations were performed using the same intensity and transit time distributions.

The results obtained for the different methods (same dataset) were compared based on the mean (time method) or central values of Gaussian fitting distributions (intensity methods). However, the standard deviation (or width) of every individual MNP distribution was not considered for this comparison, as this parameter is mostly affected by the dispersity of the MNP population and the measurement uncertainty, and thus, is independent of the method of choice for the same dataset [23,24]. Instead, uncertainties associated to the mean or central values of Gaussian fitting distributions were used for such comparison. For the calculation of these uncertainty values, an approach similar to that proposed by Yamashita et al., who evaluated the size uncertainty in SP-ICP-MS by identifying the sources of uncertainty related to the particle size method, was used [25]. In the present work, the major contributors to the uncertainty of each method were also identified and combined. This combination resulted in the equations described in the sections below, which are introduced along with a brief explanation of the measurement protocol used in each case. For more detailed information on the working principles of every approach, please refer to Section 3.

2.3.1.1. Based-on-intensity approaches

2.3.1.1.1. TE-dependent methods. As indicated above, TE-dependent methods require the prior determination of the TE for appropriate MNP sizing *via* SP-ICP-MS. Various approaches can be used for this purpose, but the most frequent ones are the particle size method and the particle frequency method, which are both based on the monitoring of MNP standards, instead of on indirect waste measurements [12].

Regarding the particle size method, MNP standards of well-known size (and, therefore, mass (m_{std})) are monitored. The signal intensities thus obtained can be processed to determine the central intensity of the Gaussian fitted distribution ($I_{c,std\ MNP}$). Therefore, the sensitivity of the MNP standards (S_{std}) in counts fg^{-1} can be calculated as the slope of a calibration curve constructed by plotting the $I_{c,std\ MNP}$ versus the m_{std}, with one or multiple standard(s) (in this case AuNPs and SiO_2MNPs). Subsequently, calibration curves prepared using appropriate concentrations of ionic standard solutions of the same target analyte as that of the MNP standards (from 0 to 5 μg L^{-1} for Au and from 0 to 10 μg L^{-1} for Si) are constructed to calculate their slope in mL fg^{-1} $counts^{-1}$ (S_{ion}). Finally, the $TE_{part.\ size}$ can be obtained in accordance with Equation (1), where $M_{std\ MNP}$ and M_{ion} are the molar mass of the standard MNP material and the ionic standard monitored, respectively, Q_{neb} is the sample uptake rate in mL min^{-1}, and t_{dwell} is the dwell time in seconds.

$$TE_{part.\ size} = \frac{M_{ion}\ S_{ion}\ 60}{M_{std\ MNP}\ Q_{neb}\ S_{std}\ t_{dwell}} \quad (1)$$

Alternatively, the particle frequency method compares the total number of events detected for an MNP standard ($N_{std\ MNP}$) of well-known PNC in mL^{-1} during a set acquisition time in seconds ($t_{acq.}$). These values can then be introduced in Equation (2) to determine the TE.

$$TE_{part.freq.} = \frac{N_{std\ MNP}\ 60}{PNC\ Q_{neb}\ t_{acq.}} \quad (2)$$

After determining the TE and regardless of the method selected (particle size or particle frequency), the integrated intensity values in counts registered for the MNP sample (I_{MNP}) can be converted to fg (m_{MNP}) according to Equation (3). In this work, the TE calculation for both the particle size and particle frequency methods was performed using all MNP standards individually (7 AuNPs and 5 SiO_2MNPs). The mass of each MNP sample was determined with an average TE calculated from the values obtained for the remaining MNPs (n = 6 for AuNPs and n = 4 for SiO_2MNPs). In other words, 7 and 5 different average TE values were calculated, excluding the TE of the MNP considered as the sample for these calculations. For the particle size method, an alternative approach was evaluated, also resulting in 7 and 5 different TE values for AuNPs and SiO_2MNPs, respectively. In this case, the difference was based on using all MNP standards except the MNP sample (n = 6 and n = 4) to calculate the slope of the calibration line required for TE calculation in the particle size method.

$$m_{MNP} = \frac{I_{MNP}\ t_{dwell}\ Q_{neb}\ TE\ M_{MNP}}{S_{ion}\ M_{ion}\ 60} \quad (3)$$

The uncertainty of the results was calculated according to Equation (4). The uptake rate was experimentally determined to estimate the $u(Q_{neb})$ as the standard deviation (n = 5). Similarly, u(TE) was determined as the standard deviation (n = 6 for AuNPs and n = 4 for SiO_2MNPs). For $u(S_{ion})$ and $u(I_{MNP})$, the standard error calculated by OriginPro for those parameters after the Gaussian fittings was used.

$$\frac{u\ (m_{MNP})}{m_{MNP}} = \sqrt{\left(\frac{u(TE)}{TE}\right)^2 + \left(\frac{u(S_{ion})}{S_{ion}}\right)^2 + \left(\frac{u(I_{MNP})}{I_{MNP}}\right)^2 + \left(\frac{u(Q_{neb})}{Q_{neb}}\right)^2} \quad (4)$$

2.3.1.1.2. TE-independent methods. TE-independent methods were based on direct external calibrations and on the adaptation of the method developed by Moreira-Álvarez et al. (relative approach) [22].

The methods based on direct external calibrations rely on (*i*) the linear correlation between intensity and mass and (*ii*) the third-degree polynomial correlation between intensity and diameter exhibited by MNPs [26]. In these approaches, the measurement protocol consists of using standard dispersions of MNPs that are well-characterized in mass and size to construct a calibration curve. In such a calibration curve, the intensities monitored for the events of MNP samples can be interpolated for determining their corresponding mass ($m_{interpol}$) and diameter ($d_{interpol}$). Analogously to the particle size and particle frequency methods, the intensities of all MNP standards were registered, but the signal of each MNP sample was always excluded for constructing the corresponding calibration curve used for its characterization. In these methods, the two main contributions to the uncertainty of the results were identified to be the interpolation of the MNP intensities in the calibration curves and the Gaussian fitting of the signal intensity distributions. For the linear approach, the uncertainty can be estimated in accordance with Equation (5), where both $u(m_{interpol})$ and $u(I_c)$ are provided by OriginPro when performing the interpolation and Gaussian fitting of sample intensities, respectively.

$$\frac{u\ (m_{MNP})}{m_{MNP}} = \sqrt{\left(\frac{u(m_{interpol})}{m_{interpol}}\right)^2 + \left(\frac{u(I_c)}{I_c}\right)^2} \quad (5)$$

For the polynomial approach, the uncertainty can be estimated according to Equation (6), where $u(d_{interpol})$ is provided by the polynomial fitting performed with OriginPro.

$$\frac{u\ (m_{MNP})}{m_{MNP}} = \sqrt{\left(3\frac{u(d_{interpol})}{d_{interpol}}\right)^2 + \left(\frac{u(I_c)}{I_c}\right)^2} \quad (6)$$

The relative approach is based on monitoring the signals obtained for AuNP and SiO_2MNP standards and those for 5 μg L^{-1} ionic standard solutions of Au and Si using the optimum voltage of the QID (set by the instrument after the daily tune). Subsequently, the instrument sensitivity was lowered by a stepwise modification of the QID value (from −10 to −18 V for Au and from −12 to −6 V for Si), registering the central intensities of the MNP fitted distributions and the average intensities of the ionic standards at every condition. Then, the method consists of plotting the relative drop in intensity for the ionic standard versus the shift of the central value in the MNP Gaussian curves (both using the optimum QID as reference). The slope of the calibration curve constructed with a standard suspension of MNPs ($S_{std\ MNP}$) of well-known size and mass ($m_{std\ MNP}$) and that of the MNP sample for which the size is to be determined (S_{MNP}) can be used to calculate the mass, according to Equation (7). Again, the calibration curve was constructed using all MNP standards, and the mass of each particle was calculated using the average of the product $m_{std\ MNP}\ S_{std\ MNP}$ obtained for the rest of the MNPs.

$$m_{MNP} = \frac{m_{std\ MNP}\ S_{std\ MNP}}{S_{MNP}} \quad (7)$$

The uncertainty of the results obtained using the relative SP-ICP-MS method can be estimated using Equation (8), where $u(m_{std\ MNP}\ S_{std\ MNP})$ was determined as the standard deviation (n = 6 for AuNPs and n = 4 for SiO_2MNPs) and $u(S_{MNP})$ was provided by the linear fitting of the sample data points performed with OriginPro. For a detailed discussion on the relative approach measurement protocol, please refer to section 3.1.2.

$$\frac{u\ (m_{MNP})}{m_{MNP}} = \sqrt{\left(\frac{u(m_{std\ MNP}\ S_{std\ MNP})}{m_{std\ MNP}\ S_{std\ MNP}}\right)^2 + \left(\frac{u(S_{MNP})}{S_{MNP}}\right)^2} \quad (8)$$

2.3.1.2. Based-on-time approach. Lastly, the analytical protocol for the based-on-time method relies on the linear correlation between the transit time (t) of the events and the MNP diameter [13]. The uncertainty of this method is primarily attributed to the interpolation on the calibration line ($d_{interpol}$), as indicated by Equation (9). The value for $u(d_{interpol})$ was provided by the linear fitting performed with OriginPro.

$$\frac{u\ (m_{MNP})}{m_{MNP}} = \sqrt{\left(3\frac{u(d_{interpol})}{d_{interpol}}\right)^2} \quad (9)$$

It should be noted that all the equations described in this section are given as a function of the particle mass. However, this work aims to compare different methodologies for MNP sizing, and thus, mass results need to be converted into size for appropriate comparison with reference values, such as those typically provided by transmission electron microscopy (TEM). For this purpose, the mass can be converted into diameter (d_{MNP}) according to Equation (10), where ρ_{MNP} is the particle density in g mL^{-1}.

$$d_{MNP} = \sqrt[3]{\frac{6}{\pi}\frac{m_{MNP}}{\rho_{MNP}}}10^4 \quad (10)$$

Following Equation (10), the relative uncertainty of MNP sizes can be estimated as a third of that calculated for the mass, given the cubic root correlation between both parameters. Then, the accuracy of each result was evaluated by comparing the experimental results with the average reference value *via* the Student's t-test at a 95 % confidence level. Please note that uncertainties of TEM analysis were not included in the statistical evaluation, as they measure the dispersity of the MNP samples and, therefore, are not comparable to those calculated in this work, where the aim was to evaluate the accuracy and uncertainty of the method for determining the central diameter of the size distribution.

2.3.2. Data processing

For processing the data exported from the Syngystix Nano Application module, the Hyper Dimensional Image Processing (HDIP v1.8.4) software was used to obtain the integrated signal intensity (peak area) of every MNP event. This software was originally designed for

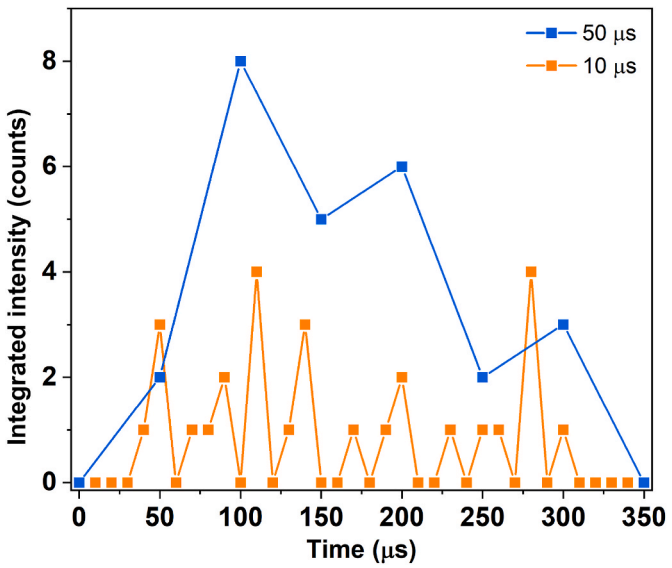

Fig. 1. Comparison between the raw data obtained for 20 nm AuNPs with dwell times of 10 and 50 µs.

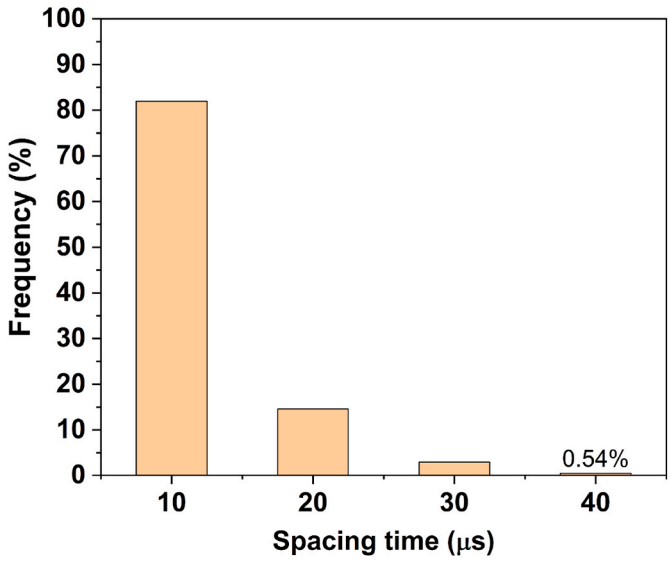

Fig. 2. Percentage of split events affected by different spacing times (N = 2233).

postprocessing of spectral data and images in the context of laser ablation (LA) – ICP-MS and is meanwhile commercially available from Teledyne Cetac Technologies for this purpose, but was adapted to identify the MNP signal events during SP-ICP-MS analysis. However, please note that most of the software packages available to date have been developed for based-on-intensity analysis [23,27–29], and most of them operate in a similar way: identifying the individual MNP events by searching for their maxima and, after that, selecting the range of integration either by looking for surrounding minima or using a fixed range in the case of well-known signal duration. These approaches are deemed suitable for based-on-intensity approaches, where small differences in the selection of the integration range barely exhibit any impact on the final intensity, as the signals of the first and last points of the event are almost negligible. Notwithstanding, those differences can be truly significant for based-on-time measurements. Consequently, an in-house Python script was developed and used throughout this work to measure the time of every individual event.

The script goes through the raw data point-by-point, searching for values above a critical one that was calculated as $\bar{x} + 2s$, where $\bar{x}$ is the mean intensity of the background, and s is the corresponding standard deviation. The 2s threshold was selected as a prefilter, followed by a second step of data depuration (see below). The script considers every data point above this threshold to be the beginning of the event. Unfortunately, identifying the end of the event is not always as simple as searching for the nearest point below the critical value. This is because when working with low dwell times (under 20 µs), as is preferable for time measurements (higher temporal resolution), the smaller MNPs whose intensity falls close to the limit of detection (LoD_{size}) may render split intensity peaks, and this would cause the underestimation of both the total intensity and duration of the event. As illustrated in Fig. 1, the total intensity of the events (sum of all of their data points: 26 and 27 counts for 50 and 10 µs, respectively) is not significantly affected by the dwell time, but split peaks are observed when increasing the data acquisition speed. On the other hand, it can also be observed that higher dwell times (lower temporal resolution) can cause a slight overestimation of the event duration.

To overcome this issue, the script only considers a point below the critical value to be the end of the MNP event if there is no other point above the threshold for the next 30 µs of signal monitoring. This selection is not random, but the result of a study carried out on more than 2000 split events. It was found that in more than 99 % of the cases, signals with intensity above the critical value corresponding to the same event were not separated by more than 30 µs, as shown in Fig. 2. Please note that it was of utmost importance not to overestimate the separation time because increasing such threshold would have caused different MNPs being detected within a narrow time window to be considered as a single event, leading to pseudo-double events.

Once the script has identified the beginning and end of the MNP event, it calculates the transit time as the product of the dwell time and the number of points belonging to that event, while the integrated intensity is calculated as the sum of the signal intensity of the points considered. As a result, the script returns a list of signal durations for each event detected, along with its corresponding integrated intensity. However, these results need to be depurated in order to eliminate data coming from double events and background signals that arise above the critical value. For this purpose, histograms were constructed from integrated intensity results, and the MNP signal distribution was fitted to a Gaussian function, so that only the event duration results associated with integrated intensities belonging to that distribution were used for the based-on-time method. The reason behind using integrated intensities (peak areas) for this depuration is that, as will be discussed later, transit time data does not always fit a Gaussian distribution and, moreover, it is feasible to obtain more information on integrated intensity distributions because the results from the in-house developed Python script can be compared with those obtained with the HDIP software.

3. Results and discussion

Before discussing the results, it is important to stress that this article is focused on sizing MNPs. The uncertainty values that will be presented and discussed throughout this work (calculated as described in 2.3.1) refer to the uncertainty in estimating the MNP size, expressed either as absolute uncertainty (u) or as relative uncertainty percentage (u%). This should not be confused with the dispersity of the MNPs, which is a different parameter.

3.1. Based-on-intensity approaches

3.1.1. TE-dependent methods

The determination of the TE values can generally be performed with one MNP standard only, but this might lead to biased conclusions when comparing these approaches with other methods for which multiple standard MNPs are measured, such as those based on direct external

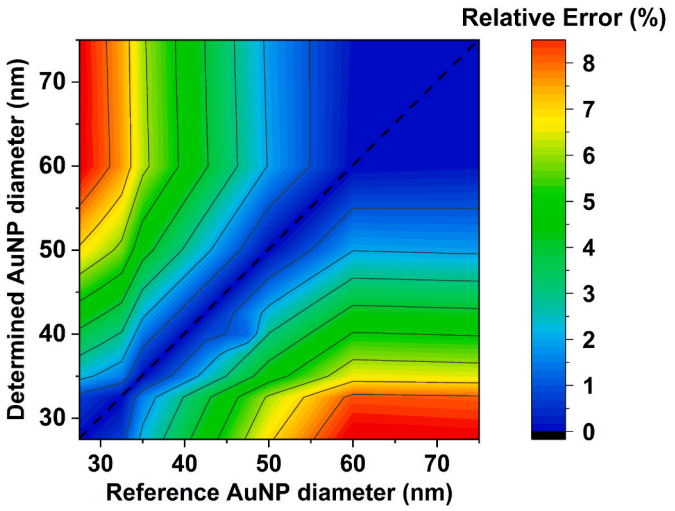

Fig. 3. Contour plot representing the relative error recorded for the particle size method when using one reference AuNP only. The dashed line corresponds to the use of the same AuNP both as sample and standard to determine the TE, leading to a null relative error regardless of the AuNP of choice.

calibration using MNP standards. Furthermore, such an MNP standard should ideally be as similar as possible to the MNP sample, both in terms of size and nature, in order to improve the accuracy of MNP sizing. As can be seen in Fig. 3, the relative error (%) in sizing AuNPs using the particle size method increased up to 8 % if the reference AuNP standard selected showed a significantly different size. However, relative errors as low as 1 % were observed when the sample-standard AuNP pairs had very similar sizes.

To overcome this limitation and to ensure a fair comparison with other methods, a TE value can be calculated using multiple MNP standards, allowing for improved size results for MNP samples of different sizes or polydisperse MNPs. Depending on the method selected, different strategies may be used, such as (*i*) calculating an average TE for both the particle frequency and particle size methods, or (*ii*) using a multipoint calibration of MNPs for the particle size method (see Fig. 4).

In this work, the results obtained for AuNPs and SiO_2MNPs using different TE calculation methods associated with the particle size method (average TE and multipoint MNP calibration TE) and the particle frequency method (average TE) were evaluated. The results are illustrated in Fig. 5, and the values obtained are also provided in Tables S1 and S2 for AuNPs and SiO_2MNPs, respectively. Please note that TE calculations were performed using 7 and 5 MNP standards for AuNPs and SiO_2MNPs, respectively. However, this approach involves using the TEs calculated for all MNP standards except that of the MNP whose size is to be determined (n-1).

As can be seen, all the approaches led to MNP sizes that were not significantly different ($p > 0.05$) from the reference sizes for both AuNPs and SiO_2MNPs. However, the particle frequency method provided results that, on average, were affected by larger uncertainties than the particle size approaches. In this regard, the average relative uncertainty (u%±SD) for the particle frequency method was 8.6 ± 0.8 % for AuNPs and 8.1 ± 1.1 % for SiO_2MNPs. In comparison, the particle size methods using an average TE or a multipoint MNP calibration TE, respectively showed an average relative uncertainty of 3.6 ± 0.4 % and 3.4 ± 0.2 % for AuNPs and 5.8 ± 0.7 % and 6.2 ± 0.5 % for SiO_2MNPs. In this context, it is also worth noting that, whereas the average relative uncertainties calculated for the particle frequency method did not significantly vary between AuNPs and SiO_2MPs, the results obtained with the particle size methods for SiO_2MNPs were affected by larger uncertainties than those obtained for AuNPs. This can be attributed to the high intensity of the Si baseline, which hinders the integration of the single events generated by SiO_2MNPs [30]. Notice that, even though the

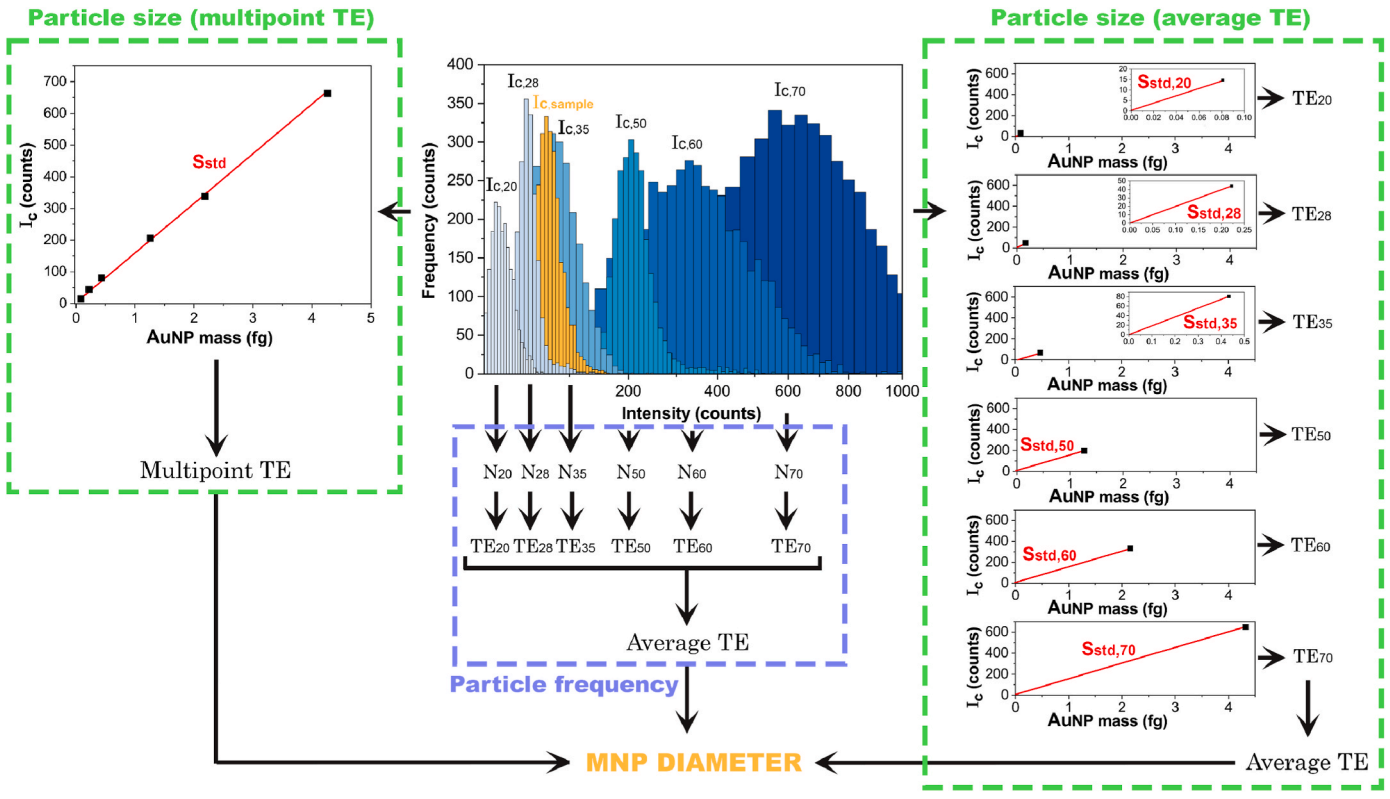

Fig. 4. Schematic representation of the different methods employed to determine the MNP diameters, exemplified for the sizing of the 32.7 nm AuNP dispersion. Please note that even though the intensity distribution was obtained for the seven AuNPs available, only the six that are not being characterized are used to determine the average or multipoint TE.

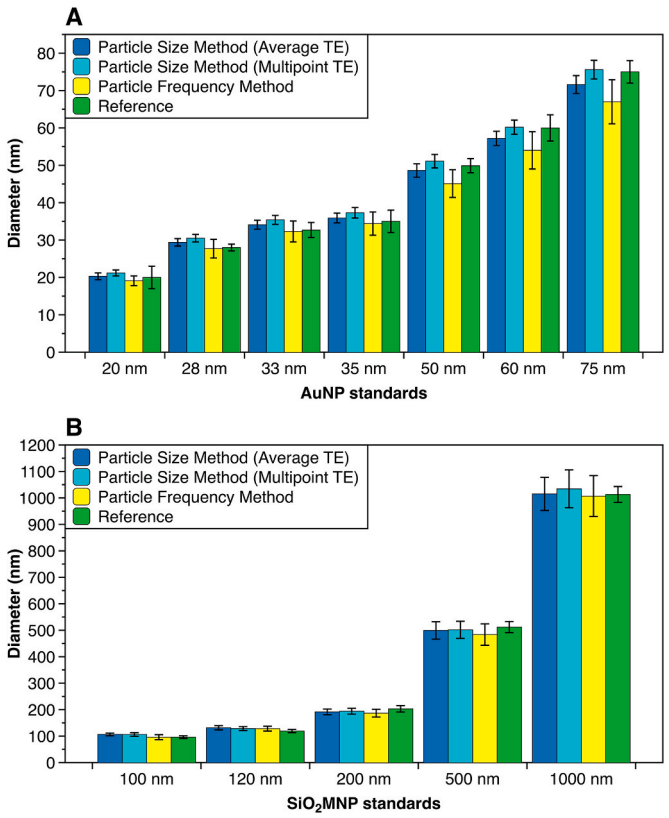

Fig. 5. Comparison of the diameters determined for different AuNPs (A) and SiO_2MNPs (B) using various TE-dependent methods with the reference values. The error bars for the three different methods compared represent the combined uncertainties (calculated as discussed in section 2.3.1.1.1.), while for the reference values the uncertainty stated in the certificate of analysis is shown.

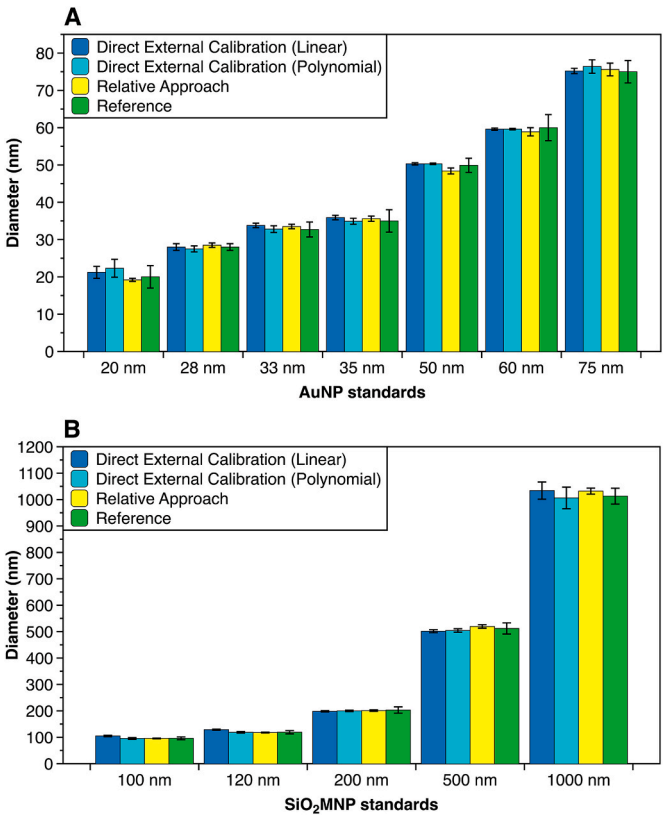

Fig. 6. Comparison of the diameters determined for the different AuNPs (A) and SiO_2MNPs (B) using various TE-independent methods with the reference values. The error bars for the three different methods compared represent the combined uncertainties (calculated as discussed in section 2.3.1.1.2.), while for the reference values the uncertainty stated in the certificate of analysis is shown.

background signal ultimately conditions both the particle size method and the particle frequency method, when it comes to determining the TE (which is the factor that governs the combined uncertainty) only the former approach relies on the monitoring of the integrated intensities of the MNP standards, and thus, it makes sense that it would be more affected by the baseline variations.

3.1.2. *TE-independent methods*

Among the different TE-independent methodologies, constructing a calibration curve with standard dispersions of MNPs of well-known mass, taking advantage of the linear correlation between the recorded integrated intensity and the MNP mass could be seen as the most straightforward approach for MNP sizing [26]. Once such a calibration curve is obtained, the intensity of any MNP event can be simply interpolated in the calibration curve to determine the corresponding MNP mass. However, this direct external calibration approach shows two main limitations: (*i*) it relies on the availability of multiple MNP standards of different sizes and, (*ii*) those standards should ideally be distributed evenly along the curve, so that all of them have the same weight on the calibration, thus minimizing biased results [31]. The first limitation is becoming progressively less important since the MNP market grows in response to the growing interest in the field, although the relatively high purchase cost may still limit access to such standards, and, thus, jeopardize the applicability of this methodology. Moreover, the purchase of MNPs of evenly distributed masses is not an easy task because the cubic relationship between mass and size entails that MNPs of relatively close sizes are, in reality, very different in terms of MNP mass. Furthermore, MNPs are typically produced to achieve a certain size, not a certain mass.

The impact of this limitation is clearly observed when comparing the size results obtained for AuNPs and those for SiO_2MNPs (see Fig. 6 and Tables S3 and S4).

In this context, no significant differences at the 95 % confidence level were observed for AuNPs when comparing the experimental sizes with the reference values, whereas the linear calibration did not succeed for sizing the smaller SiO_2MNPs, displaying significant differences at the 95 % confidence level for results obtained with the standards of 100 nm and 120 nm. This can be attributed to the more evenly scattered AuNP standards, given the greater commercial availability and the smaller range of sizes to be covered. Conversely, SiO_2MNPs standards show vast differences in terms of mass between them, as illustrated in Fig. 7. Therefore, the integrated signal intensities obtained for the larger SiO_2MNPs governed the calibration, jeopardizing both the accuracy and precision at the lower range of the curve. An average relative uncertainty of 2.3 ± 2.5 % and 1.6 ± 1.0 % (u%±SD) was calculated for the AuNPs (n = 7) and the SiO_2MNPs (n = 5), respectively. It is noteworthy that, while the average relative uncertainty is lower than that of other methods, it exhibits higher dispersity (expressed as SD). The reason for this observation is that the uncertainty linked to calibration through a linear regression is enhanced from the center of the curve to the edges [31], being especially boosted when the I_c value falls outside the calibration range, as shown in Fig. 7. In this context, the average relative uncertainty was decreased to 1.4 ± 1.2 % for AuNPs (n = 5) and 0.9 ± 0.7 % (n = 3) for SiO_2MNPs upon excluding the extreme data points. Therefore, this technique seems to be more adequate when pursuing the analysis of MNP samples of mass within the range covered by the MNP standards, as typically occurs with all external calibration approaches.

To circumvent the dispersed distribution of MNP standards that characterize linear regressions, it is possible to take advantage of the

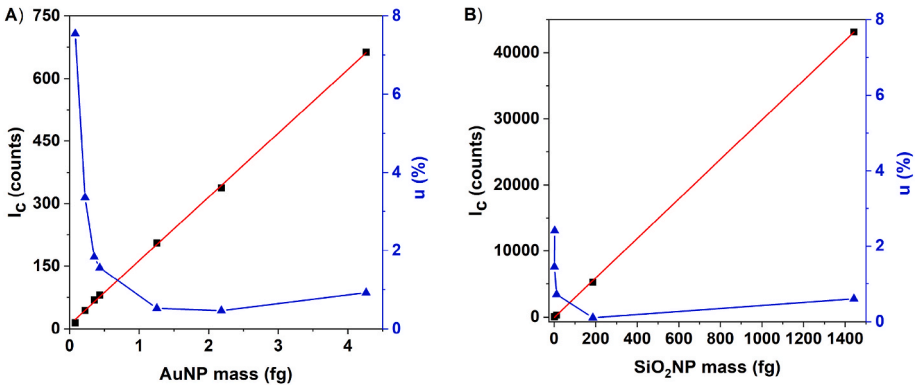

Fig. 7. Representation of the linear calibration curves (squares, left y-axis) and of the relative uncertainty in the MNP mass (triangles, right y-axis) for (A) AuNPs and (B) SiO_2MNPs.

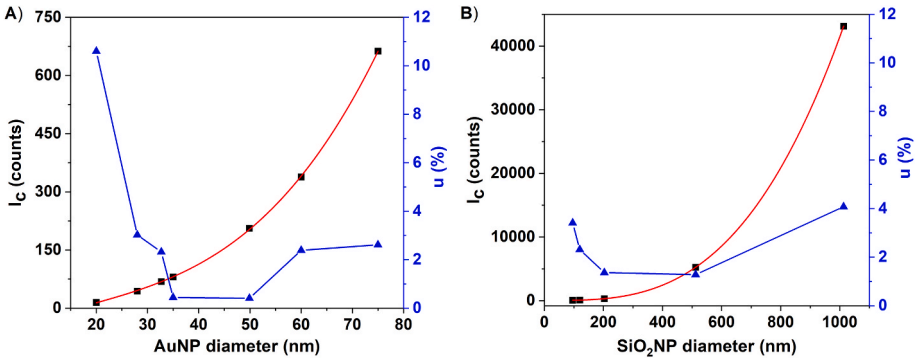

Fig. 8. Representation of the third-degree polynomial calibration curves (squares, left y-axis) and of the relative uncertainty in the MNP diameter (triangles, right y-axis) for (A) AuNPs and (B) SiO_2MNPs.

cubic relationship between the recorded integrated intensity and the MNP size, which allows for the calibration with a third-degree polynomial function. As previously discussed, differences in MNP size are less sharp than for MNP mass, so it should be easier to find evenly distributed standards while using this calibration strategy. Therefore, the same MNP standards that were very dispersed for the linear calibration are more equally spread with the polynomial approach, as illustrated in Fig. 8. As a result, no significant differences at the 95 % confidence level were found for the results obtained using this approach as compared to the reference values for both kinds of MNPs. An average relative uncertainty of 3.1 ± 3.5 % and 2.5 ± 1.2 % (u%±SD) was calculated for AuNPs (n = 7) and SiO_2MNPs (n = 5), respectively. Again, extreme points, whose I_c values fall outside the calibration range, exhibit abnormally high u%, causing the overestimation of the average uncertainty, as shown in Fig. 8. However, for MNP samples whose sizes fall within the calibration range, the u%±SD improved down to 1.7 ± 1.2 % and 1.6 ± 0.6 % for AuNPs (n = 5) and SiO_2MNPs (n = 3), achieving size results that are equivalent to those obtained with the linear relationship in terms of uncertainty, but with improved accuracy. Finally, it should be acknowledged that, whereas at least two data points are required for a linear fitting, no less than four data points must be represented to identify the third-degree polynomial function that adjusts well to the experimental data, which reveals the main limitation of this methodology. In this context, five different SiO_2MNP standards were monitored in this work, so that calibration curves were constructed with only four MNP standards, given that the MNP to characterize (sample) was not included in the calibrations. This is enough to identify the fitting function for the interpolation; however, analogously to linear fittings constructed with two data points only, it is not possible to estimate the uncertainty of the third-degree polynomial interpolation if only four MNP standards are used, as the regression coefficient R^2 is equal to 1. Therefore, the intercept of the function was fixed to 0, given that an MNP of no size would theoretically render no intensity, to determine the uncertainty of the interpolations ($u(d_{interpol})$).

Similarly to the polynomial calibration strategy, the relative approach developed by Moreira-Álvarez et al. [22] also achieves calibration curves with evenly distributed data points. Additionally, it requires a single MNP standard only, circumventing the two restrictions of the linear particle calibration method. As previously introduced, this method consists of analyzing an ionic standard, an MNP standard of well-known mass, and the MNP sample at different instrumental conditions providing different sensitivity. In the original article [22], the lens voltages were the parameters tuned to modify the sensitivity. However, the ICP-MS instrument used in this work is not fitted with a lens interface but with a quadrupole ion deflector (QID), and thus, the QID voltages were modified to implement this approach. After measuring every standard at each QID voltage, a calibration curve was constructed with every MNP standard by plotting the relative drop of ionic intensity versus the shift of the mean intensity for the MNP standard distributions, as it is schematized in Fig. 9. Therefore, this methodology assumes that the same relative drop of intensity is occurring both for MNP standards and for ionic standard solutions so that, by plotting one against the other, data points should align to a curve with a slope of 1. However, since we are not plotting the relative drop for MNPs but the intensity shift (which represents the numerator of the relative drop equation), the slope of the curve (S_{MNP}) corresponds to the reciprocal of the MNP intensity at the optimum conditions (I_1), which is the denominator of the relative drop equation. Therefore, this approach determines the optimum intensity of both the MNP standard and the sample through the construction of a calibration curve with the measurements performed at different sensitivity conditions, rather than with a single measurement. Then, the particle mass of the MNP sample can be

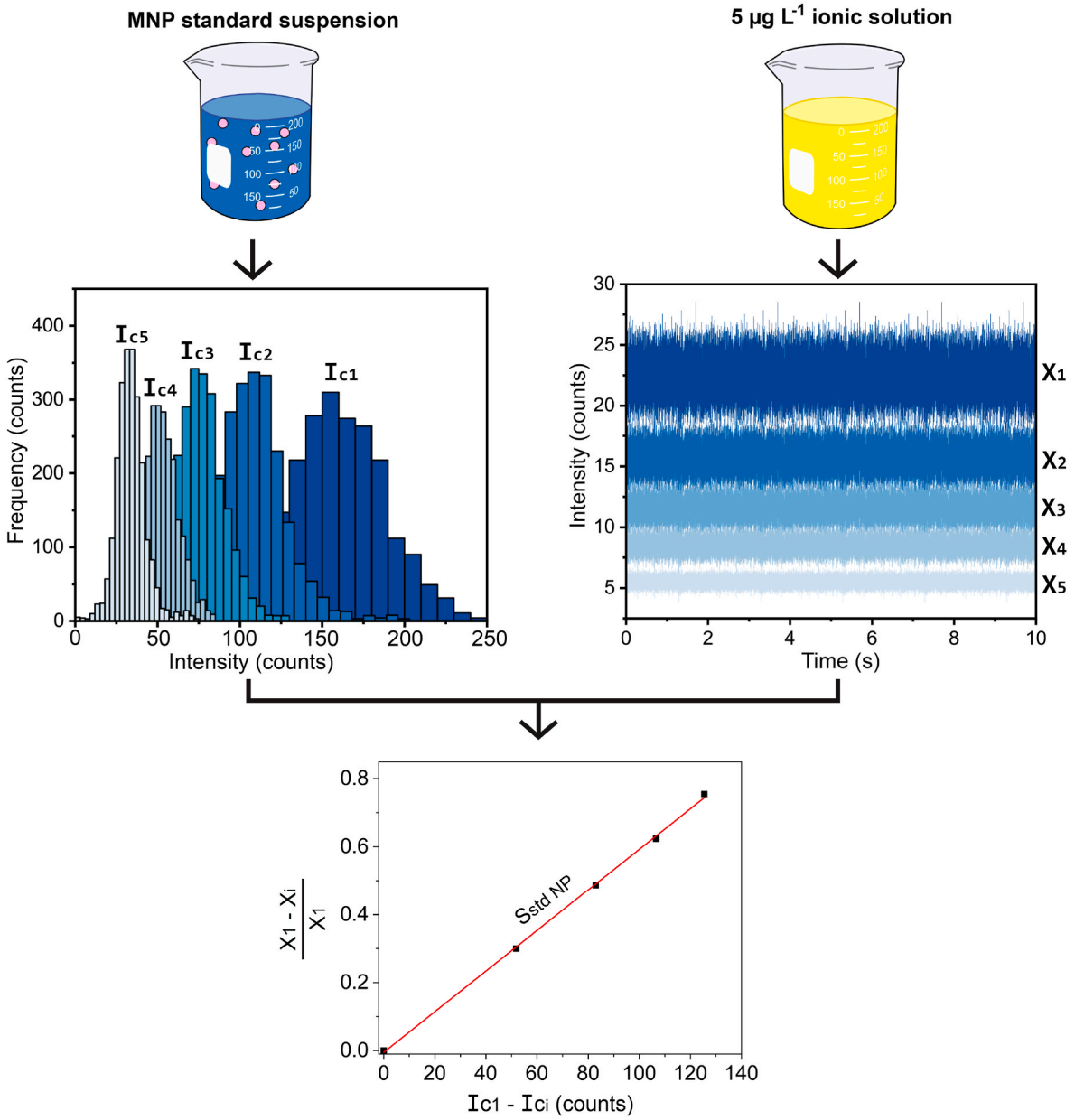

Fig. 9. Schematic representation of the protocol derived from the work of Moreira-Álvarez et al. [22] followed to obtain the calibration curve. Subindexes represent different sensitivity conditions (1 being the optimum). X_i and I_{ci} are, respectively, the average intensity of the ionic standard and the central intensity of the fitted Gaussian of the MNP standard at each sensitivity condition.

calculated given that the ratio m_{MNP}/I_1 (*i.e.*, $m_{MNP}S_{NP}$) is constant for every MNP, as discussed in Section 2.3.1.1.2. As to the results, no significant difference in terms of size was observed for any MNP, and the average uncertainty (u%±SD) was calculated to be 2.0 ± 0.2 % and 1.3 ± 0.2 % for AuNPs (n = 7) and SiO_2MNPs (n = 5), respectively, which represents an uncertainty level comparable to the rest of the TE-independent approaches, but with less dispersion. However, it should be noted that the main drawback of this approach is inherent to the necessity of monitoring MNPs under progressively less sensitive conditions, which jeopardizes its applicability to MNPs of sizes close to the LoD_{size} (as calculated when operating under optimum conditions).

3.2. Based-on-time approach

As previously mentioned, the application of transit time measurements on the characterization of MNP sizes is very similar to the linear external calibration discussed among the based-on-intensity approaches. However, by monitoring the duration of individual events, analytical signals can be linearly correlated with the MNP size directly, rather than with the MNP mass, *a priori* circumventing the limitation of MNP standards not being uniformly distributed along the calibration curve, as in polynomial calibrations. Additionally, monitoring the time offers the advantage of being unaffected by sensitivity fluctuations of the instrument during the working session (as long as the method is not applied to sizes close to the LoD_{size}), which could be very significant given the fact that internal standards are not usually deployed during SP-ICP-MS analysis due to obvious duty cycle limitations [24].

Self-evidently, selecting an adequate dwell time is of the utmost importance when pursuing the determination of the transit time of single events. In this regard, the use of lower dwell times (i.e., faster data acquisition speeds) should increase the accuracy with which the beginning and end of each event can be identified. However, lowering

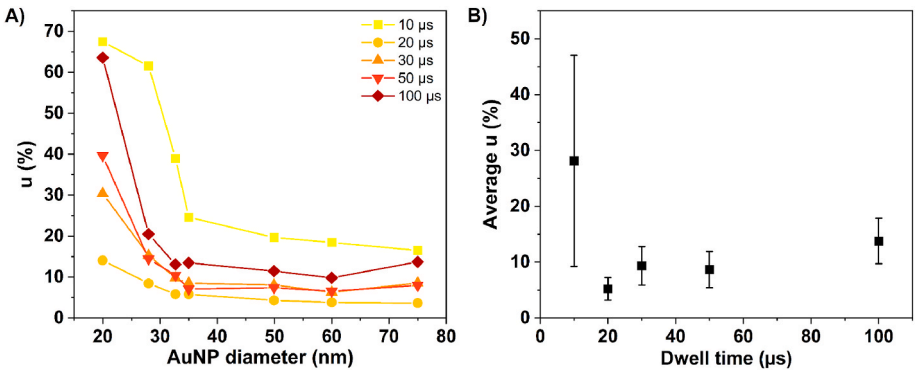

Fig. 10. (A) Evolution of the calculated u% as a function the AuNP size. (B) Evolution of the average u% with the selected dwell time. Error bars represent the SD of the u%.

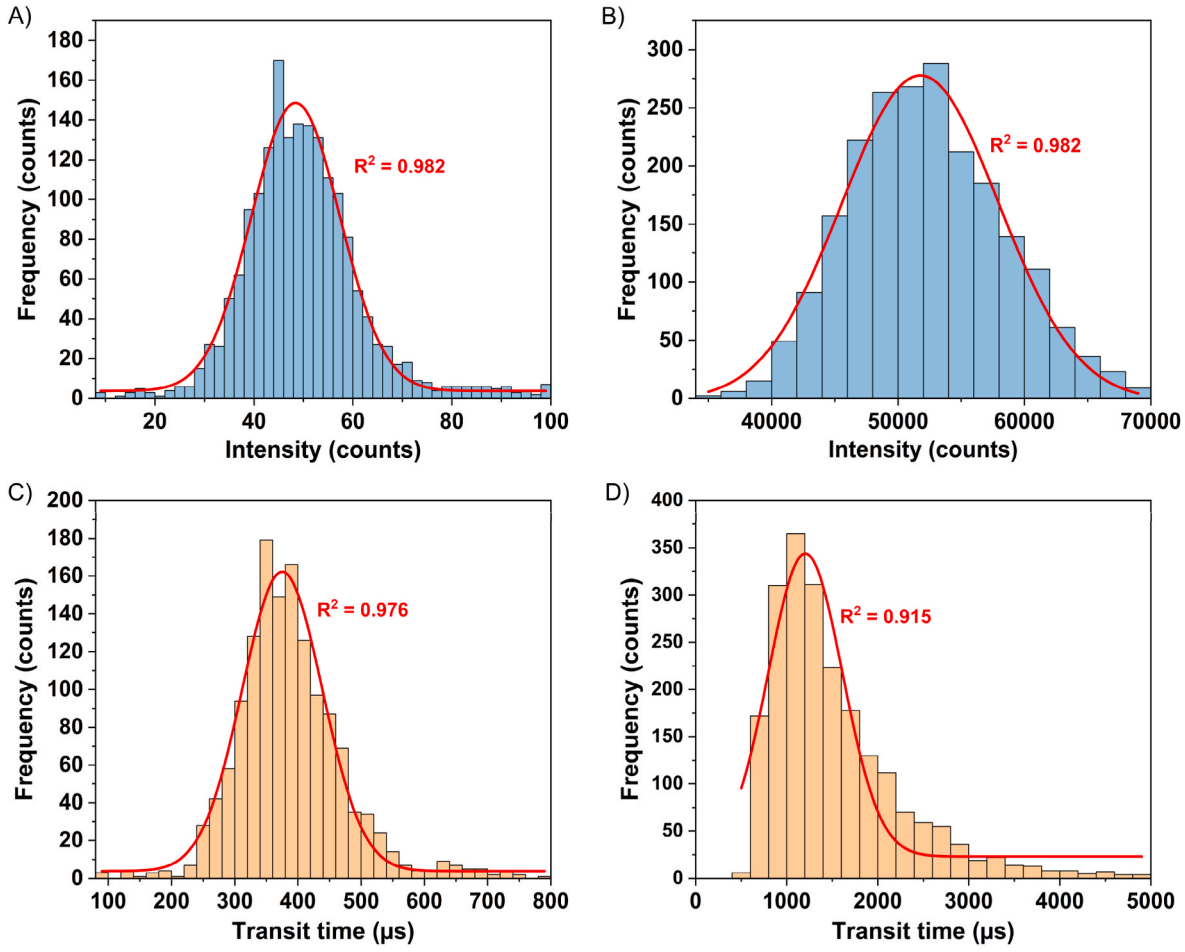

Fig. 11. Comparison between intensity (A and B) and transit time (C and D) distributions for 30 nm AuNPs (A and C) and 1000 nm SiO_2MNPs (B and D).

the dwell time also lowers the intensity of each data point, as the same integrated signal intensity is being split into more data points, which negatively impacts the LoD_{size}. Therefore, there is a compromise between accuracy and LoD_{size} that needs to be considered before selecting the dwell time for any given application. In this case, all the evaluated MNPs were analyzed at five different dwell times (10, 20, 30, 50, and 100 µs) to identify the optimum value for each MNP type. Since the method relies on high temporal resolution, the use of longer dwell times would strongly compromise its applicability. Fig. 10 shows how the uncertainty for the results obtained with this method for the AuNPs was affected both by the size of the NP to be characterized (A) and by the dwell time selected (B). As to the effect of the MNP size, the accuracy of the method (expressed as u%) significantly improves as the MNP size increases for all dwell times (Fig. 10A). This can be attributed to the higher intensities, increasing the contrast between the background and the event data points and lowering the uncertainty associated with the identification of the beginning and end points. However, for large enough particles (MNP diameters above 35 nm), the accuracy of the method remains fairly constant. On the other hand, the lowest and least dispersed average u% value was obtained with a dwell time of 20 µs (Fig. 10B). Thus, this dwell time was selected for the analysis of AuNPs. In contrast, the results obtained with a dwell time of 10 µs clearly

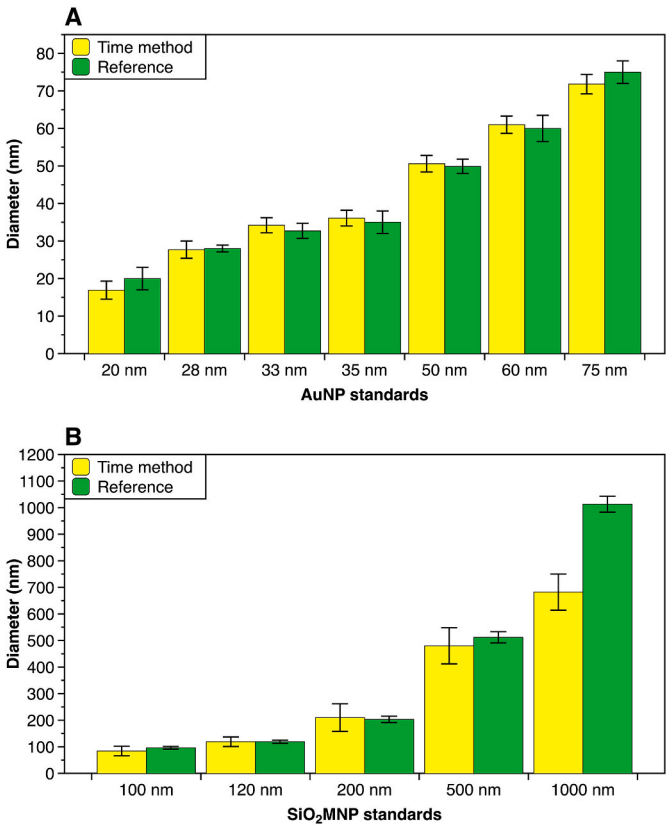

Fig. 12. Comparison of the diameters determined for the different AuNPs (A) and SiO_2MNPs (B) using the time method with the reference values. The error bars for the time method represent the combined uncertainties (calculated as discussed in section 2.3.1.2.), while for the reference values the uncertainty stated in the certificate of analysis is shown. The dwell time was set at 20 μs and 100 μs for AuNPs and SiO_2MNPs, respectively.

exemplify how further lowering the dwell time below the optimum value, far from improving the accuracy as a result of a higher temporal resolution, hinders the determination of the transit time for small MNPs, and negatively impacts the calibration and, as a result, the overall uncertainty for sizing. Turning to SiO_2MNPs, given the lower sensitivity and the presence of an intense background that jeopardizes the identification of the boundaries of the MNP events, enough signal-to-noise contrast to detect all the five MNPs available could only be achieved with a dwell time of 100 μs, which was selected for further analysis of SiO_2MNPs.

For the based-on-intensity approaches, data processing consisted of fitting the signal intensity distributions into Gaussian functions, and the adjusted central value was used to construct the MNP calibrations (Fig. 11A and B). However, when the transit time is tracked, the smaller MNPs adjust to Gaussians (Fig. 11C), whereas the bigger ones exhibit a positive-tailed distribution (Fig. 11D). Therefore, different data points of the same calibration adjust to different functions. As a result, the average transit time was the parameter chosen to build the calibration curves, thus avoiding making assumptions about the function to which the distributions were adjusted. The apparition of the tail only for bigger MNPs can most likely be attributed to different diffusion and mixing processes of the ion clouds generated upon MNP digestion during their passage through the plasma, which results in the extension of the transit times [13,21]. In this context, big MNPs need more time to be fully digested, and thus, only some of them have enough time to fully expand. This variation in the expansion of MNPs will result in several distributions (e.g., various Gaussian distributions centered on different transit times), appearing overall as a convoluted distribution showing a marked tail (see Fig. 11D). This phenomenon represents one of the main

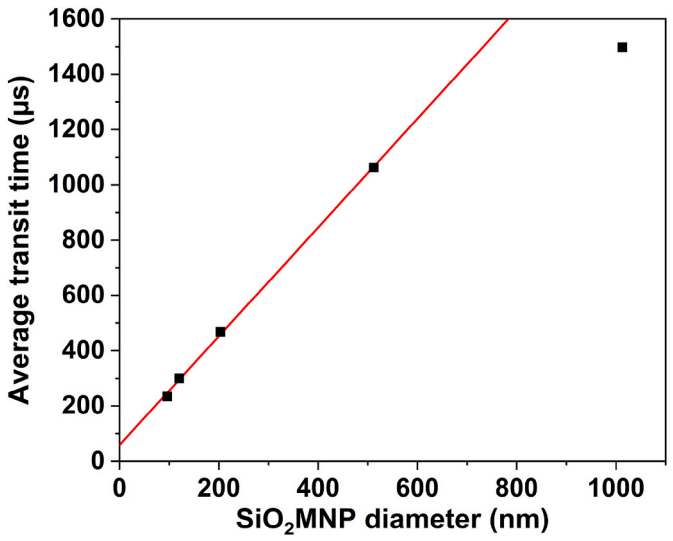

Fig. 13. Evolution of the transit time with the SiO_2MNP size along with the linear correlation observed for the first four data points.

downsides of the time method, which is the inability to obtain the accurate mass or size distributions of relatively big MNPs, rendering the average size the only achievable information.

The results obtained for AuNPs and SiO_2MNPs with the dwell times selected are shown in Fig. 12 and Tables S5 and S6. For AuNPs, no significantly different sizes at a 95 % confidence level were determined for any MNP in comparison to the reference values, and an average uncertainty of 6.5 ± 3.7 % (u%±SD, n = 7) was obtained. Analogously to the based-on-intensity linear calibration, this average u% can be improved down to 5.2 ± 2.0 % if the results of the extreme points (which are obtained for transit time values that fall outside the calibration range) are not considered, which is comparable to the values obtained with the particle size method. However, a significantly different size was obtained for the SiO_2MNP standard of 1000 nm. As evidenced in Fig. 13, the data point corresponding to the MNPs of 1000 nm SiO_2 is clearly out of the linear range, which explains the difference as compared to the reference value. One may think that this observation indicates that bigger SiO_2MNPs are not being completely digested in the plasma, but, if that were the case, the same effect should have been evidenced for the intensity calibration. Nevertheless, it is also true that a *quasi*-complete digestion may have a negligible impact on the intensity, but a more significant one on the transit time, so this phenomenon could indeed contribute to this outlier behavior. Another explanation is related to the different diffusion and mixing processes that expand the transit time, as already discussed before: large MNPs need more time to be fully digested, and thus, those processes do not occur to the same extent as for smaller MNPs, leading to abnormally narrow events. Therefore, the SiO_2MNPs of 1000 nm were not introduced in any calibration to avoid biasing the results. As to the accuracy, an average uncertainty of 17.2 ± 6.0 % (u%±SD, n = 4) was found, which represents the worst value among the different methods evaluated in this work. This relatively high uncertainty as compared to that observed for AuNPs can probably be related to the presence of a high background signal and to the fact that a relatively high dwell time of 100 μs (low temporal resolution) had to be used. Additionally, it should be mentioned that H_2 was introduced into the CRC to overcome the spectral interference of $(^{12}C^{16}O)^+$ and $(^{14}N^{14}N)^+$ on $^{28}Si^+$, which has been reported to entail the broadening of the duration of the events [32,33], and that might also be negatively affecting the overall uncertainty values. Notwithstanding, the impact of this effect is not expected to be very important given the small size of the H_2 molecule and the relatively low gas flow rate used (0.9 mL min^{-1}).

Table 2
Summary of the conclusions and results achieved for each one of the methods evaluated.

Method	u% ± SD		Observations
	AuNPs	SiO_2MNPs	
Particle size (average TE)	3.6 ± 0.4	5.8 ± 0.7	+ Only a single MNP standard is required (as similar as possible to the sample) - Uncertainty affected by the background
Particle size (multipoint TE)	3.4 ± 0.2	6.2 ± 0.5	- Uncertainty affected by the background
Particle frequency	8.6 ± 0.8	8.1 ± 1.1	+ Uncertainty is less affected by the background - Higher uncertainty than other approaches
Direct external calibration (linear fit)	1.4 ± 1.2	0.9 ± 0.7	+ Simpler calculations - Optimum accuracy only for events that fall inside of the calibration range - Multiple MNP standards are required
Direct external calibration (polynomial fit)	1.7 ± 1.2	1.6 ± 0.6	+ Simpler calculations - At least four MNP standards are required
Relative approach	2.0 ± 0.2	1.3 ± 0.2	+ Only one MNP standard is required - Sizing of MNPs close to the LoD is compromised
Time method	5.2 ± 2.0	17.2 ± 6.0	+ Signal directly related to size, not to mass + Less affected by sensitivity fluctuations of the instrument + It opens possibilities to differentiate among nanomaterials of different shapes and compositions [10,11] - For optimum results, instruments with low dwell times are required - Size distribution possible only for small MNPs - Shorter linear range

4. Conclusions

In this work, the performance of different based-on-intensity and based-on-time methods for sizing AuNPs and SiO_2MNPs was evaluated, comparing the accuracy of the size results obtained with the different methods and their applicability. In general, all the methods that were evaluated succeeded in sizing the different MNP standards, which ratifies that more than one approach can be evaluated for any application intended. Therefore, carefully considering the different strengths and weaknesses of the different methods may greatly improve the quality of the SP-ICP-MS measurement results.

The main conclusions obtained for each approach are summarized in Table 2. In short, the best accuracy is achieved with TE-independent based-on-intensity methods (*i.e.,* direct external calibration and the relative approach developed by Moreira-Álvarez et al. [22]), although they are associated with other limitations such as the need for multiple MNP standards or greater inaccuracy in characterizing MNPs whose I_c falls outside the calibration range. In contrast, other approaches, such as the particle frequency method and the based-on-time method, might provide results affected by larger uncertainties, but they offer other benefits such as being unaffected by the background or by sensitivity fluctuations during the working session. Finally, the particle size method offers the most accurate results, provided that an appropriate single MNP standard is selected or multiple MNP standards are used. This justifies why this is currently the most widely implemented approach for sizing MNPs *via* SP-ICP-MS. Nevertheless, as instruments displaying more sensitivity and higher temporal resolution are released, and highly monodispersed MNPs standards become readily available, the advantages offered by other approaches should also be considered.

Finally, it is deemed important to stress that the current work is focused only on sizing MNPs. Determining the particle number concentration is certainly also possible using SP-ICP-MS, but it requires different considerations [12].

CRediT authorship contribution statement

Antonio Bazo: Writing – review & editing, Writing – original draft, Visualization, Validation, Methodology, Investigation, Formal analysis, Data curation, Conceptualization. **Eduardo Bolea-Fernandez:** Writing – review & editing, Supervision, Project administration, Conceptualization. **Ana Rua-Ibarz:** Writing – review & editing, Supervision, Conceptualization. **Maite Aramendía:** Writing – review & editing, Supervision, Project administration, Conceptualization. **Martín Resano:** Writing – review & editing, Supervision, Resources, Project administration, Funding acquisition, Conceptualization.

Declaration of competing interest

The authors declare that they have no known competing financial interests or personal relationships that could have appeared to influence the work reported in this paper.

Data availability

Data will be available through Zenodo

Acknowledgements

The authors are grateful to the European Regional Development Fund ("ERDF A way of making Europe") for financial support through the Interreg POCTEFA Nanolyme EFA99/1, to project PID2021-122455NB-I00 (funded by MCIN/AEI/10.13039/501100011033 and by ERDF) and also to the Aragon Government (DGA, Construyendo Europa desde Aragón, Grupo E43_20R). A.B. acknowledges the Department of Science, University and Knowledge Society from DGA his predoctoral grant (2021 call). E.B.-F. acknowledges financial support from the Ramón y Cajal programme (RYC2021-031093-I) funded by MCIN/AEI/10.13039/501100011033 and the European Union (NextGenerationEU/PRTR). A.R.-I. thanks European Union's Horizon 2020 research and innovation program under the Marie-Sklodowska-Curie grant agreement Nº 101034288. M. Mataloni and L. López-Villellas are also acknowledged for their support.

Appendix A. Supplementary data

Supplementary data to this article can be found online at https://doi.org/10.1016/j.aca.2024.343305.

References

[1] J. Vidmar, R. Milačič, J. Ščančar, Sizing and simultaneous quantification of nanoscale titanium dioxide and a dissolved titanium form by single particle inductively coupled plasma mass spectrometry, Microchem. J. 132 (2017) 391–400, https://doi.org/10.1016/j.microc.2017.02.030.

[2] M.E. Johnson, S.K. Hanna, A.R. Montoro Bustos, C.M. Sims, L.C.C. Elliott, A. Lingayat, A.C. Johnston, B. Nikoobakht, J.T. Elliott, R.D. Holbrook, K.C.K. Scott, K.E. Murphy, E.J. Petersen, L.L. Yu, B.C. Nelson, Separation, sizing, and quantitation of engineered nanoparticles in an organism model using inductively coupled plasma mass spectrometry and image analysis, ACS Nano 11 (2017) 526–540, https://doi.org/10.1021/acsnano.6b06582.

[3] R. Gonzalez de Vega, T.E. Lockwood, X. Xu, C. Gonzalez de Vega, J. Scholz, M. Horstmann, P.A. Doble, D. Clases, Analysis of Ti- and Pb-based particles in the aqueous environment of Melbourne (Australia) via single particle ICP-MS, Anal. Bioanal. Chem. 414 (2022) 5671–5681, https://doi.org/10.1007/s00216-022-04052-0.

[4] J. Vidmar, L. Hässmann, K. Loeschner, Single-particle ICP–MS as a screening technique for the presence of potential inorganic nanoparticles in food, J. Agric. Food Chem. 69 (2021) 9979–9990, https://doi.org/10.1021/acs.jafc.0c07363.
[5] K. Loeschner, M.E. Johnson, A.R. Montoro Bustos, Application of single particle ICP-MS for the determination of inorganic nanoparticles in food additives and food: a short review, Nanomaterials 13 (2023) 2547, https://doi.org/10.3390/nano13182547.
[6] S. Fernández-Trujillo, M. Jiménez-Moreno, Á. Ríos, R. del C. Rodríguez Martín-Doimeadios, A simple analytical methodology for platinum nanoparticles control in complex clinical matrices via SP-ICP-MS, Talanta 231 (2021) 122370, https://doi.org/10.1016/j.talanta.2021.122370.
[7] S. Mourdikoudis, R.M. Pallares, N.T.K. Thanh, Characterization techniques for nanoparticles: comparison and complementarity upon studying nanoparticle properties, Nanoscale 10 (2018) 12871–12934, https://doi.org/10.1039/C8NR02278J.
[8] T. Van Acker, S. Theiner, E. Bolea-Fernandez, F. Vanhaecke, G. Koellensperger, Inductively coupled plasma mass spectrometry, Nat Rev Methods Primers 3 (2023) 1–18, https://doi.org/10.1038/s43586-023-00235-w.
[9] C. Degueldre, P.-Y. Favarger, Colloid analysis by single particle inductively coupled plasma-mass spectroscopy: a feasibility study, Colloids Surf. A Physicochem. Eng. Asp. 217 (2003) 137–142, https://doi.org/10.1016/S0927-7757(02)00568-X.
[10] B. Meermann, V. Nischwitz, ICP-MS for the analysis at the nanoscale – a tutorial review, J. Anal. At. Spectrom. 33 (2018) 1432–1468, https://doi.org/10.1039/C8JA00037A.
[11] D. Mozhayeva, C. Engelhard, A critical review of single particle inductively coupled plasma mass spectrometry – a step towards an ideal method for nanomaterial characterization, J. Anal. At. Spectrom. 35 (2020) 1740–1783, https://doi.org/10.1039/C9JA00206E.
[12] M. Resano, M. Aramendía, E. García-Ruiz, A. Bazo, E. Bolea-Fernandez, F. Vanhaecke, Living in a transient world: ICP-MS reinvented via time-resolved analysis for monitoring single events, Chem. Sci. 13 (2022) 4436–4473, https://doi.org/10.1039/D1SC05452J.
[13] I. Kálomista, A. Kéri, D. Ungor, E. Csapó, I. Dékány, T. Prohaska, G. Galbács, Dimensional characterization of gold nanorods by combining millisecond and microsecond temporal resolution single particle ICP-MS measurements, J. Anal. At. Spectrom. 32 (2017) 2455–2462, https://doi.org/10.1039/C7JA00306D.
[14] A. Kéri, I. Kálomista, D. Ungor, Á. Bélteki, E. Csapó, I. Dékány, T. Prohaska, G. Galbács, Determination of the structure and composition of Au-Ag bimetallic spherical nanoparticles using single particle ICP-MS measurements performed with normal and high temporal resolution, Talanta 179 (2018) 193–199, https://doi.org/10.1016/j.talanta.2017.10.056.
[15] A.M. Duffin, E.D. Hoegg, R.I. Sumner, T. Cell, G.C. Eiden, L.S. Wood, Temporal analysis of ion arrival for particle quantification, J. Anal. At. Spectrom. 36 (2021) 133–141, https://doi.org/10.1039/D0JA00412J.
[16] A. Schardt, J. Schmitt, C. Engelhard, Single particle inductively coupled plasma mass spectrometry with nanosecond time resolution, J. Anal. Atomic Spectrom. 39 (2024) 389–400, https://doi.org/10.1039/D3JA00373F.
[17] H.E. Pace, N.J. Rogers, C. Jarolimek, V.A. Coleman, C.P. Higgins, J.F. Ranville, Determining transport efficiency for the purpose of counting and sizing nanoparticles via single particle inductively coupled plasma mass spectrometry, Anal. Chem. 83 (2011) 9361–9369, https://doi.org/10.1021/ac201952t.
[18] E. Bolea, F. Laborda, Single particle inductively coupled plasma mass spectrometry metrology: revisiting the transport efficiency paradigm, Spectrochim. Acta B Atom Spectrosc. 216 (2024) 106941, https://doi.org/10.1016/j.sab.2024.106941.
[19] A. Gustavsson, The determination of some nebulizer characteristics, Spectrochim. Acta B Atom Spectrosc. 39 (1984) 743–746, https://doi.org/10.1016/0584-8547(84)80159-7.
[20] S. Cuello-Nuñez, I. Abad-Álvaro, D. Bartczak, M.E. del Castillo Busto, D.A. Ramsay, F. Pellegrino, H. Goenaga-Infante, The accurate determination of number concentration of inorganic nanoparticles using spICP-MS with the dynamic mass flow approach, J. Anal. Atom. Spectrom. 35 (2020) 1832–1839, https://doi.org/10.1039/C9JA00415G.
[21] M.D. Montaño, J.W. Olesik, A.G. Barber, K. Challis, J.F. Ranville, Single Particle ICP-MS: advances toward routine analysis of nanomaterials, Anal. Bioanal. Chem. 408 (2016) 5053–5074, https://doi.org/10.1007/s00216-016-9676-8.
[22] B. Moreira-Álvarez, L. Cid-Barrio, F. Calderón-Celis, J.M. Costa-Fernández, J. R. Encinar, Relative and transport efficiency-independent approach for the determination of nanoparticle size using single-particle ICP-MS, Anal. Chem. 95 (2023) 10430–10437, https://doi.org/10.1021/acs.analchem.3c01823.
[23] M. Aramendía, J.C. García-Mesa, E.V. Alonso, R. Garde, A. Bazo, J. Resano, M. Resano, A novel approach for adapting the standard addition method to single particle-ICP-MS for the accurate determination of NP size and number concentration in complex matrices, Anal. Chim. Acta 1205 (2022) 339738, https://doi.org/10.1016/j.aca.2022.339738.
[24] A. Bazo, M. Aramendía, F.V. Nakadi, M. Resano, An approach based on an increased bandpass for enabling the use of internal standards in single particle ICP-MS: application to AuNPs characterization, Nanomaterials 13 (2023) 1838, https://doi.org/10.3390/nano13121838.
[25] S. Yamashita, S. Miyashita, T. Hirata, Size uncertainty in individual nanoparticles measured by single particle inductively coupled plasma mass spectrometry, Nanomaterials 13 (2023) 1958, https://doi.org/10.3390/nano13131958.
[26] A.R. Montoro Bustos, K.P. Purushotham, A. Possolo, N. Farkas, A.E. Vladár, K. E. Murphy, M.R. Winchester, Validation of single particle ICP-MS for routine measurements of nanoparticle size and number size distribution, Anal. Chem. 90 (2018) 14376–14386, https://doi.org/10.1021/acs.analchem.8b03871.
[27] G. Cornelis, M. Hassellöv, A signal deconvolution method to discriminate smaller nanoparticles in single particle ICP-MS, J. Anal. At. Spectrom. 29 (2013) 134–144, https://doi.org/10.1039/C3JA50160D.
[28] J. Tuoriniemi, G. Cornelis, M. Hassellöv, A new peak recognition algorithm for detection of ultra-small nano-particles by single particle ICP-MS using rapid time resolved data acquisition on a sector-field mass spectrometer, J. Anal. At. Spectrom. 30 (2015) 1723–1729, https://doi.org/10.1039/C5JA00113G.
[29] T.E. Lockwood, R.G. de Vega, D. Clases, An interactive Python-based data processing platform for single particle and single cell ICP-MS, J. Anal. At. Spectrom. 36 (2021) 2536–2544, https://doi.org/10.1039/D1JA00297J.
[30] E. Bolea-Fernandez, D. Leite, A. Rua-Ibarz, L. Balcaen, M. Aramendía, M. Resano, F. Vanhaecke, Characterization of SiO2 nanoparticles by single particle-inductively coupled plasma-tandem mass spectrometry (SP-ICP-MS/MS), J. Anal. At. Spectrom. 32 (2017) 2140–2152, https://doi.org/10.1039/C7JA00138J.
[31] J.N. Miller, J.C. Miller, R.D. Miller, Statistics and Chemometrics for Analytical Chemistry, seventh ed., Pearson, International, 2018. https://www.pearson.de/statistics-and-chemometrics-for-analytical-chemistry-9781292186726. (Accessed 28 May 2024).
[32] E. Bolea-Fernandez, D. Leite, A. Rua-Ibarz, T. Liu, G. Woods, M. Aramendia, M. Resano, F. Vanhaecke, On the effect of using collision/reaction cell (CRC) technology in single-particle ICP-mass spectrometry (SP-ICP-MS), Anal. Chim. Acta 1077 (2019) 95–106, https://doi.org/10.1016/j.aca.2019.05.077.
[33] A. Rua-Ibarz, E. Bolea-Fernandez, G. Pozo, X. Dominguez-Benetton, F. Vanhaecke, K. Tirez, Characterization of iron oxide nanoparticles by means of single-particle ICP-mass spectrometry (SP-ICP-MS) – chemical versus physical resolution to overcome spectral overlap, J. Anal. At. Spectrom. 35 (2020) 2023–2032, https://doi.org/10.1039/D0JA00183J.